

# Vision Mamba for Classification of Breast Ultrasound Images

Ali Nasiri-Sarvi<sup>1</sup>, Mahdi S. Hosseini<sup>1</sup>, and Hassan Rivaz<sup>2</sup>

<sup>1</sup> Department of Computer Science and Software Engineering (CSSE), Concordia University, Canada

<sup>2</sup> Department of Electrical and Computer Engineering (ECE), Concordia University, Canada

**Abstract.** Mamba-based models, VMamba and Vim, are a recent family of vision encoders that offer promising performance improvements in many computer vision tasks. This paper compares Mamba-based models with traditional Convolutional Neural Networks (CNNs) and Vision Transformers (ViTs) using the breast ultrasound BUSI dataset and Breast Ultrasound B dataset. Our evaluation, which includes multiple runs of experiments and statistical significance analysis, demonstrates that some of the Mamba-based architectures often outperform CNN and ViT models with statistically significant results. For example, in the B dataset, the best Mamba-based models have a 1.98% average AUC and a 5.0% average Accuracy improvement compared to the best non-Mamba-based model in this study. These Mamba-based models effectively capture long-range dependencies while maintaining some inductive biases, making them suitable for applications with limited data. The code is available at <https://github.com/anasiri/BU-Mamba>.

**Keywords:** Vision Mamba · State Space Models · Breast Ultrasound, Breast Cancer

## 1 Introduction

Processing breast ultrasound images using deep learning can benefit from pre-trained weights and a transfer learning paradigm, especially when dealing with smaller datasets [1]. Several factors influence the effectiveness of transfer learning. One crucial factor is the choice of the pretrained dataset [2], and another critical factor is the selection of the encoder architecture [2].

Convolutional Neural Networks (CNNs) [3] and Vision Transformers (ViTs) [4, 5] have been studied for breast ultrasound applications in works such as [6–8]. Recently, a new family of encoders, Vim [9] and VMamba [10], based on State Space Models (SSMs), has emerged in computer vision, leveraging the Mamba architecture [11]. Although studies like UMamba [12] have recently investigated the Mamba architecture for medical imaging dataset segmentation, its performance in breast ultrasound classification has yet to be explored.

In this work, we adopt these architectures from natural image processing, utilizing pretrained weights trained on ImageNet [13], and compare them with

common CNN and ViT architectures on two breast ultrasound datasets, BUSI [14] and B dataset [15]. We also conduct a statistical analysis to ensure that the performance improvements are significant. Our results show that Mamba-based architectures frequently outperform other encoder types with significant results. They are also never outperformed by the other encoders in terms of statistical significance.

## 2 Related Work

CNNs [3] have shown tremendous capability in computer vision tasks, with AlexNet [16] achieving breakthrough performance in the ImageNet Challenge [13], leading to widespread adoption of deep learning models in the field with models such as ResNet [17] and VGG [18]. While CNNs excel at capturing local patterns, they are limited in capturing long-range dependencies due to their limited receptive field.

ViTs [4, 5] have been proposed as an alternative to CNN models. They generally outperform these CNN models due to a lack of inductive bias present in CNNs, allowing ViT models to freely learn from the dataset using the attention mechanism [19, 20] and effectively capture long-range dependencies. However, this lack of inductive bias also means these models require more data and training to achieve similar performance to CNNs or outperform them.

Recently, a new family of architectures based on the Mamba model [11] has emerged, leveraging State Space Models (SSMs) in deep learning [21]. These architectures, including VMamba [10] and Vision Mamba (Vim) [9], show potential in various applications like video understanding [22], remote sensing [23], pathology datasets [24], and point clouds [25]. In medical imaging, Mamba-based models have demonstrated significant potential, particularly for segmentation tasks, as explored in [12, 26–29].

We aim to do a comparative analysis between the Mamba-based models compared to CNN and ViT architectures on two widely adopted breast ultrasound datasets BUSI [14] and B dataset [15]. Since these datasets are small, our analysis uses transfer learning for the comparison. Similar work on comparative analysis for CNN and ViT has been explored for breast ultrasound datasets. For example, the impact of transfer learning on CNNs for breast ultrasound images is explored in [6, 7, 30]. In [8], ViTs are compared to CNNs through transfer learning. Our goal is to extend these studies to Mamba-based models.

## 3 Preliminaries

In this section, we provide an overview of the state space models. These preliminaries would help with understanding the Mamba model.

### 3.1 State Space Models

State space models are mathematical frameworks that describe continuous linear systems. The state equation defines how the state  $h(t)$  evolves as a function of the input  $x(t)$ , as shown in Eq. 1.

$$h_t = Ah_{t-1} + Bx_t \quad (1)$$

The output equation links the connection between the output, the hidden state, and the input based on Eq. 2.

$$y_t = Ch_t + Dx_t \quad (2)$$

The parameters  $A$ ,  $B$ , and  $C$  are time-invariant and remain unchanged across the sequence in the S4 model [21]. This time-invariance allows using a global convolution to represent the sequential data, thereby avoiding the slowdown typically seen in recurrent modeling. The global convolution for a sequence of length  $L$  is defined based on the Eq. 3 ( $\overline{CAB}$  is used to showcase discretized parameters):

$$y = \bar{K} * x \quad (3)$$

$$\bar{K} \in \mathbb{R} := \mathcal{K}_L(A, B, C) = (\overline{CB}, \overline{CAB}, \dots, \overline{CA^{L-1}B})$$

Although this time-invariance accelerates processing speed, it restricts the model’s ability to behave dynamically based on each input token, thus constraining its overall performance.

### 3.2 Mamba

In Mamba [11], selective state spaces are used where the state space parameters  $B$ ,  $C$ , and  $\Delta$  (a discretization parameter) are computed dynamically based on each input sequence, with  $A$  as the only time-invariant parameter. This dependence on the input improves the model’s ability to capture temporal variations and complex dependencies in the data. However, this dependence on the input prevents the option of using a global convolution, limiting the ability to utilize the parallel processing capabilities of GPUs due to the recurrent processing.

Mamba uses a hardware-aware algorithm to increase the processing speed, considering that modern GPUs have two types of memory, SRAM and HBM, with the first being faster but having less capacity. Since the parameter  $A$  is still time-invariant, they move it to the fast SRAM for the sequential processing. At each time step, they compute  $B$ ,  $C$ , and  $\Delta$  in HBM and move  $B$  and  $\Delta$  to SRAM to compute the state space recurrence. The state vectors are then moved to HBM to compute the output based on Eq. 2 using the previously computed  $C$ . This hardware-aware algorithm makes Mamba’s throughput a sequential model comparable to parallel transformers.

## 4 Methods

In this section, we explain two vision models based on Mamba Architecture.

### 4.1 Vim

In Vim, images are divided into smaller patches, each projected into a patch embedding. A bidirectional Mamba processes these patches by considering both previous and next tokens. Additionally, positional encoding is added to each token to retain spatial information about neighboring patches. The architecture is illustrated in Fig 1. Vim has similar processing to ViT models but uses Mamba-based blocks instead of attention-based Transformer blocks.

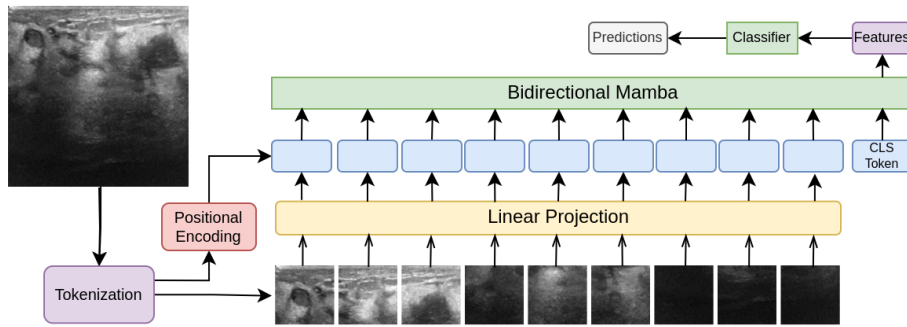


Fig. 1. An over view of the Vim model

### 4.2 VMamba

VMamba introduces “2D Selective Scan” to the Mamba’s original scan. Furthermore, instead of breaking the image into tokens and processing each token similarly to ViT and Vim, the image patches are treated as feature maps and are processed using VSS blocks similar to CNN models, where the feature maps are down-sampled at each layer. The overall pipeline is demonstrated in Fig. 2.

### 4.3 Model Comparison

Fig. 3 shows how different encoders process images. In CNNs, if patches P1 and P2 do not fall in the same receptive field, the model will struggle to capture long-range dependencies. In the ViT model, the attention mechanism would allow the model to process the relationship between P1 and P9. However, distinguishing between pairs like P1-P2 and P1-P9 relies primarily on positional encoding. As a result, the model needs more data and training to differentiate these pairs

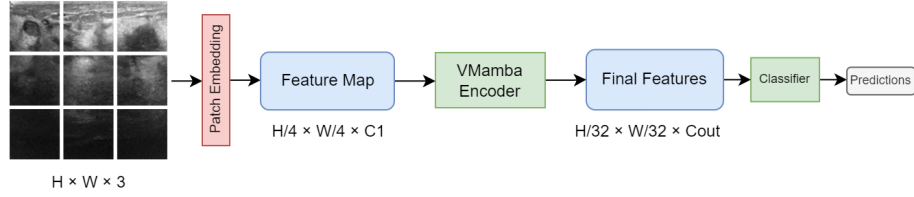


**Fig. 2.** An over view of the VMamba model

accurately and focus on close-range dependencies. This increased demand for training arises from the absence of the inductive bias, where neighboring patches are assumed to have similar content.

In Mamba-based models, the inductive bias is reintroduced through Mamba’s sequential processing, similar to models like PixelRNN [31]. However, unlike PixelRNN, Mamba allows for long-range information processing and more efficiently utilizes GPUs. Consequently, Mamba-based models combine CNNs’ inductive bias with ViT’s long-range processing capability, offering the best of both worlds.

When comparing Vim and VMamba, Vim uses a bidirectional Mamba scan to achieve multi-directional feature extraction across the patches. In contrast, VMamba’s 2D selective Scan employs the Mamba scan in four directions to capture more comprehensive and complex relationships between the image patches, enhancing the feature representation and in-context learning.

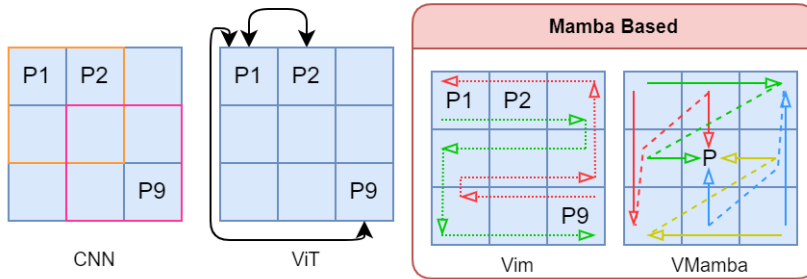


**Fig. 3.** An abstract comparison between different architecture types.

## 5 Experiments

This section summarizes the performance of various encoder types on different datasets. For our classification task, we use the BUSI [14] dataset (three classes of benign, malignant, and normal), the Dataset B of [15] (two classes of benign and malignant), and a combined BUSI+B dataset (three classes of normal,

benign, and malignant). Each table reports the Area Under the Curve (AUC), Accuracy (ACC) metrics, and the number of parameters for each encoder. Since the experiment datasets are imbalanced, AUC is required as a more valuable metric. For BUSI and BUSI+B, which have three classes, the AUC is calculated individually for each class by comparing it against the other two classes. The final AUC for an experiment is then determined by averaging these individual AUC scores.

We use ResNet50 [17] and VGG16 [18] as the CNN-based models. For ViT models, we use ViT-ti16, ViT-s16, ViT-s32, ViT-b16, and ViT-b32 [4], where the prefixes 'ti,' 's,' and 'b' denote tiny, small, and base model sizes, respectively, and the numbers indicate the patch size used (16x16 or 32x32 pixels). For Mamba-based models, we use Vim-s16 [9], VMamba-ti, VMamba-s, and VMamba-b [10]. These Mamba-based models have the default parameters and definition as provided in the papers. We use pretrained weights of each of these encoders from ImageNet for transfer learning.

We conduct each experiment across five training runs, using different seeds to minimize randomness in experiments. The data is split into training, validation, and test sets with respective splits of 0.7, 0.15, and 0.15. The validation set is used for early stopping; we select the checkpoint that shows the best performance on the validation set to prevent overfitting to the test set. Results are reported based on the test set's performance for each fold.

We assess statistical significance between two encoders using a paired t-test on their prediction. This analysis is conducted across all five folds, using the checkpoints from each model trained on the training set of a fold and subsequently tested on the test set.

## 5.1 Results on the BUSI+B Dataset

The classification performance of Mamba-based and ViT/CNN models is provided in Table 1. We ran our experiments five times and averaged the results to obtain mean and standard deviation measurements. Mamba-based models achieve higher or comparable results to ViT and CNN models. However, the high variance in the results and the small dataset size necessitate statistical significance analysis to compare the results.

**Statistical Significance Analysis:** To further evaluate the differences in performance between Mamba-based models and ViT/CNN models on the BUSI + B dataset, statistical tests are conducted using t-tests, and the threshold for the  $p$ -value is set to 0.05. The  $p$ -values were computed by comparing the accuracy of predictions between two models and testing for a zero mean difference.

This analysis reveals that VMamba-ti outperforms VGG16 (p-value: 0.004), ViT-ti16 (p-value: 0.003), ViT-s32 (p-value: 0.014), and ViT-b32 (p-value: 0.022), and the difference is significant. VMamba-b outperforms VGG16 (p-value: 0.037) and ViT-ti16 (p-value: 0.015). Additionally, ViT-b16 performs better than VGG16 (p-value: 0.044) and ViT-ti16 (p-value: 0.013). There are no other significant differences between pairs of models (the p-value is bigger than 0.05). This showcases

**Table 1.** Transfer Learning Results for BUSI+B datasets. The values of AUC and ACC are scaled between 0 to 100. The results are averaged over five runs.

Encoder Type	Encoder	# Params (Millions)	BUSI+B	
			AUC	ACC
CNN	ResNet50	23.5	$95.74 \pm 1.42$	$87.66 \pm 2.04$
	VGG16	134.3	$94.25 \pm 1.28$	$85.82 \pm 1.49$
ViT	ti-16	5.5	$94.19 \pm 1.74$	$85.39 \pm 1.93$
	s-16	21.7	$95.39 \pm 0.54$	$87.23 \pm 2.33$
	s-32	22.5	$93.85 \pm 0.72$	$86.24 \pm 1.65$
	b-16	85.8	$95.76 \pm 0.77$	$88.51 \pm 2.67$
	b-32	87.5	$95.51 \pm 1.53$	$86.52 \pm 3.23$
Vim	s-16	25.4	$95.84 \pm 0.96$	$87.38 \pm 3.22$
VSSM	VMamba-ti	29.9	$95.71 \pm 1.01$	$89.36 \pm 2.33$
	VMamba-s	49.4	$96.12 \pm 0.75$	$87.80 \pm 2.78$
	VMamba-b	87.5	$95.60 \pm 0.79$	$88.51 \pm 2.22$

that Mamba-based models perform similarly or outperform other encoders on the BUSI+B dataset with respect to statistical significance.

It is important to note that while ResNet50, as shown in Table 1, achieves a higher mean AUC of 95.74 compared to some of the other models, the statistical significance analysis indicates that this improvement is not significant. For example, when testing for ResNet50 against ViT-s32, the p-value is 0.27, even though the mean AUC and ACC for ResNet50 are better. Due to the experiments’ small dataset size and inherent randomness, we report both mean and standard deviation for each metric, which makes direct comparisons between models more complex. Therefore, statistical analysis is necessary to reduce this randomness and better identify instances where the differences between pairs of models are statistically significant and not due to randomness in the experiments.

## 5.2 Results on the BUSI Dataset

The classification results for the BUSI dataset are provided in Table 2. We ran our experiments five times and averaged the results to obtain the mean and standard deviation measurements. The results suggest that the Mamba-based models outperform the other encoders on the B dataset.

**Statistical Significance:** We performed  $p$ -value tests on the BUSI dataset. The analysis demonstrates that ViT-b16, VMamba-s, and Vim-s outperform ViT-s32 (with a  $p$ -value of 0.036, 0.027, and 0.011, respectively). VMamba-ti model outperforms ResNet50 ( $p$ -value: 0.032), VGG16 ( $p$ -value: 0.024), and ViT-s32 ( $p$ -value: 0.002). The VMamba-b model notably surpasses ResNet50 ( $p$ -value: 0.015), VGG16 ( $p$ -value: 0.006), ViT-ti16 ( $p$ -value: 0.018), ViT-s16 ( $p$ -value: 0.022), ViT-s32 ( $p$ -value: 0.0001), and ViT-b32 ( $p$ -value: 0.029). There are no other pairs with  $p$ -values smaller than 0.05. These results indicate that the Mamba-based models frequently performed at or above the level of other models with respect to statistical significance.

**Table 2.** Transfer Learning Results for BUSI dataset. The values of AUC and ACC are scaled between 0 to 100. The results are averaged over five runs.

Encoder Type	Encoder	# Params (Millions)	BUSI	
			AUC	ACC
CNN	ResNet50	23.5	93.23 $\pm$ 1.93	85.64 $\pm$ 2.72
	VGG16	134.3	93.69 $\pm$ 2.18	85.47 $\pm$ 4.59
ViT	ti-16	5.5	93.52 $\pm$ 3.07	85.98 $\pm$ 4.48
	s-16	21.7	93.60 $\pm$ 4.04	86.50 $\pm$ 4.44
	s-32	22.5	93.59 $\pm$ 2.59	84.10 $\pm$ 3.81
	b-16	85.8	94.11 $\pm$ 2.12	87.18 $\pm$ 2.70
	b-32	87.5	94.10 $\pm$ 1.23	85.98 $\pm$ 1.39
Vim	s-16	25.4	95.63 $\pm$ 1.66	87.86 $\pm$ 2.72
VSSM	VMamba-ti	29.9	95.28 $\pm$ 1.89	88.55 $\pm$ 1.67
	VMamba-s	49.4	94.48 $\pm$ 3.48	87.18 $\pm$ 4.15
	VMamba-b	87.5	94.67 $\pm$ 2.53	89.06 $\pm$ 3.72

### 5.3 Results on the B Dataset

The classification results for the B dataset are provided in Table 3. We conducted our experiments five times and calculated the average and standard deviation of the results. VMamba-ti is the best model, outperforming all other encoders on average AUC and having a large margin on average ACC. Other Mamba encoders also perform competitively and often surpass other models.

**Table 3.** Transfer Learning Results for B dataset. The values of AUC and ACC are scaled between 0 to 100. The results are averaged over five runs.

Encoder Type	Encoder	# Params (Millions)	B	
			AUC	ACC
CNN	ResNet50	23.5	90.05 $\pm$ 4.19	78.33 $\pm$ 5.53
	VGG16	134.3	88.24 $\pm$ 7.10	80.00 $\pm$ 6.67
ViT	ti-16	5.5	80.90 $\pm$ 9.98	77.50 $\pm$ 7.26
	s-16	21.7	90.68 $\pm$ 7.89	82.50 $\pm$ 6.67
	s-32	22.5	87.55 $\pm$ 8.89	79.17 $\pm$ 9.50
	b-16	85.8	88.32 $\pm$ 6.24	76.67 $\pm$ 7.26
	b-32	87.5	83.14 $\pm$ 12.82	77.50 $\pm$ 12.25
Vim	s-16	25.4	87.42 $\pm$ 9.83	84.17 $\pm$ 8.50
VSSM	VMamba-ti	29.9	92.66 $\pm$ 9.07	87.50 $\pm$ 12.08
	VMamba-s	49.4	88.70 $\pm$ 9.30	83.33 $\pm$ 10.54
	VMamba-b	87.5	92.19 $\pm$ 5.43	81.67 $\pm$ 6.24

**Statistical Significance:** Our statistical significance analysis for the B dataset reveals that ViT-s16 outperforms ViT-b16 (p-value: 0.034). Vim-s performs better than both ViT-ti16 (p-value: 0.032) and ViT-b16 (p-value: 0.019). VMamba-ti model shows remarkable performance by outperforming ResNet50



(p-value: 0.011), VGG16 (p-value: 0.028), ViT-ti16 (p-value: 0.004), ViT-s32 (p-value: 0.012), ViT-b16 (p-value: 0.003), ViT-b32 (p-value: 0.007), and even VMamba-b (p-value: 0.034). There are no other pairs of models with p-values smaller than 0.05. These results underscore VMamba-ti as the top performer among the models evaluated. Furthermore, there are no instances with statistical significance where non-Mamba-based models outperformed Mamba-based models.

## 6 Discussion

The overall performance on the three datasets demonstrates the advantages of using Mamba-based models for breast cancer ultrasound datasets. Additionally, Mamba-based models’ ability to capture long-range dependencies while retaining some inductive bias makes them a suitable alternative to CNN and ViT models, especially in scenarios with limited data and resources. Furthermore, VMamba showed better performance overall compared to Vim. This could be due to 2D selective scan of VMamba, which allows better representation learning.

One limitation of this study is that the statistical significance analysis is not considering the imbalance in the dataset due the multi-class analysis and complexity of comparing AUC for pairs of models. Despite this, some Mamba-based models frequently have higher average AUC as provided in the experiments section. A more comprehensive statistical analysis, including the multi-class AUC, would provide stronger support for our results.

## 7 Conclusion

In this work, we conducted a comprehensive comparison of three families of vision encoders—ViT, CNN, and Mamba-based models—using the BUSI and B datasets and a combined BUSI+B dataset. Our evaluation included multiple runs, averages, and standard deviations, and we performed a statistical significance analysis for each experiment. Overall, Mamba-based models frequently demonstrated competitive performance compared to the other models, with statistically significant results. Additionally, they were never outperformed by any other encoder type regarding statistical significance.

**Acknowledgments.** This project was funded by the Natural Sciences and Engineering Research Council of Canada (NSERC) and Fonds de recherche du Québec – Nature et technologies (FRQNT). We also extend our gratitude to Behnaz Gheflati for their valuable time.

**Disclosure of Interests.** The authors have no competing interests to declare that are relevant to the content of this article.

## References

1. K. Yasaka, H. Akai, A. Kunimatsu, S. Kiryu, and O. Abe, "Deep learning with convolutional neural network in radiology," *Japanese journal of radiology*, vol. 36, pp. 257–272, 2018.
2. F. Zhuang, Z. Qi, K. Duan, D. Xi, Y. Zhu, H. Zhu, H. Xiong, and Q. He, "A comprehensive survey on transfer learning," *Proceedings of the IEEE*, vol. 109, no. 1, pp. 43–76, 2020.
3. Y. Lecun and Y. Bengio, "Convolutional networks for images, speech, and time-series," 01 1995.
4. A. Dosovitskiy, L. Beyer, A. Kolesnikov, D. Weissenborn, X. Zhai, T. Unterthiner, M. Dehghani, M. Minderer, G. Heigold, S. Gelly, *et al.*, "An image is worth 16x16 words: Transformers for image recognition at scale," *arXiv preprint arXiv:2010.11929*, 2020.
5. H. Touvron, M. Cord, M. Douze, F. Massa, A. Sablayrolles, and H. Jégou, "Training data-efficient image transformers & distillation through attention," in *International conference on machine learning*, pp. 10347–10357, PMLR, 2021.
6. J. F. Lazo, S. Moccia, E. Frontoni, and E. De Momi, "Comparison of different cnns for breast tumor classification from ultrasound images," *arXiv preprint arXiv:2012.14517*, 2020.
7. W. Al-Dhabyani, M. Gomaa, H. Khaled, and F. Aly, "Deep learning approaches for data augmentation and classification of breast masses using ultrasound images," *Int. J. Adv. Comput. Sci. Appl.*, vol. 10, no. 5, pp. 1–11, 2019.
8. B. Gheflati and H. Rivaz, "Vision transformers for classification of breast ultrasound images," in *2022 44th Annual International Conference of the IEEE Engineering in Medicine & Biology Society (EMBC)*, pp. 480–483, IEEE, 2022.
9. L. Zhu, B. Liao, Q. Zhang, X. Wang, W. Liu, and X. Wang, "Vision mamba: Efficient visual representation learning with bidirectional state space model," *arXiv preprint arXiv:2401.09417*, 2024.
10. Y. Liu, Y. Tian, Y. Zhao, H. Yu, L. Xie, Y. Wang, Q. Ye, and Y. Liu, "Vmamba: Visual state space model," *arXiv preprint arXiv:2401.10166*, 2024.
11. A. Gu and T. Dao, "Mamba: Linear-time sequence modeling with selective state spaces," *arXiv preprint arXiv:2312.00752*, 2023.
12. J. Ma, F. Li, and B. Wang, "U-mamba: Enhancing long-range dependency for biomedical image segmentation," *arXiv preprint arXiv:2401.04722*, 2024.
13. J. Deng, W. Dong, R. Socher, L.-J. Li, K. Li, and L. Fei-Fei, "Imagenet: A large-scale hierarchical image database," in *2009 IEEE conference on computer vision and pattern recognition*, pp. 248–255, Ieee, 2009.
14. W. Al-Dhabyani, M. Gomaa, H. Khaled, and A. Fahmy, "Dataset of breast ultrasound images," *Data in brief*, vol. 28, p. 104863, 2020.
15. M. H. Yap, G. Pons, J. Marti, S. Ganau, M. Sentis, R. Zwigelaar, A. K. Davison, and R. Marti, "Automated breast ultrasound lesions detection using convolutional neural networks," *IEEE journal of biomedical and health informatics*, vol. 22, no. 4, pp. 1218–1226, 2017.
16. A. Krizhevsky, I. Sutskever, and G. E. Hinton, "Imagenet classification with deep convolutional neural networks," *Advances in neural information processing systems*, vol. 25, 2012.
17. K. He, X. Zhang, S. Ren, and J. Sun, "Deep residual learning for image recognition," in *Proceedings of the IEEE conference on computer vision and pattern recognition*, pp. 770–778, 2016.

18. K. Simonyan and A. Zisserman, "Very deep convolutional networks for large-scale image recognition," *arXiv preprint arXiv:1409.1556*, 2014.
19. D. Bahdanau, K. Cho, and Y. Bengio, "Neural machine translation by jointly learning to align and translate," *arXiv preprint arXiv:1409.0473*, 2014.
20. A. Vaswani, N. Shazeer, N. Parmar, J. Uszkoreit, L. Jones, A. N. Gomez, Ł. Kaiser, and I. Polosukhin, "Attention is all you need," *Advances in neural information processing systems*, vol. 30, 2017.
21. A. Gu, K. Goel, and C. Ré, "Efficiently modeling long sequences with structured state spaces," *arXiv preprint arXiv:2111.00396*, 2021.
22. K. Li, X. Li, Y. Wang, Y. He, Y. Wang, L. Wang, and Y. Qiao, "Videomamba: State space model for efficient video understanding," *arXiv preprint arXiv:2403.06977*, 2024.
23. K. Chen, B. Chen, C. Liu, W. Li, Z. Zou, and Z. Shi, "Rsmamba: Remote sensing image classification with state space model," *IEEE Geoscience and Remote Sensing Letters*, 2024.
24. A. Nasiri-Sarvi, V. Q.-H. Trinh, H. Rivaz, and M. S. Hosseini, "Vim4path: Self-supervised vision mamba for histopathology images," in *Proceedings of the IEEE/CVF Conference on Computer Vision and Pattern Recognition (CVPR) Workshops*, pp. 6894–6903, June 2024.
25. J. Liu, R. Yu, Y. Wang, Y. Zheng, T. Deng, W. Ye, and H. Wang, "Point mamba: A novel point cloud backbone based on state space model with octree-based ordering strategy," *arXiv preprint arXiv:2403.06467*, 2024.
26. W. Liao, Y. Zhu, X. Wang, C. Pan, Y. Wang, and L. Ma, "Lightm-unet: Mamba assists in lightweight unet for medical image segmentation," *arXiv preprint arXiv:2403.05246*, 2024.
27. J. Ruan and S. Xiang, "Vm-unet: Vision mamba unet for medical image segmentation," *arXiv preprint arXiv:2402.02491*, 2024.
28. Z. Wang, J.-Q. Zheng, Y. Zhang, G. Cui, and L. Li, "Mamba-unet: Unet-like pure visual mamba for medical image segmentation," *arXiv preprint arXiv:2402.05079*, 2024.
29. Z. Xing, T. Ye, Y. Yang, G. Liu, and L. Zhu, "Segmamba: Long-range sequential modeling mamba for 3d medical image segmentation," *arXiv preprint arXiv:2401.13560*, 2024.
30. M. Amiri, R. Brooks, and H. Rivaz, "Fine-tuning u-net for ultrasound image segmentation: different layers, different outcomes," *IEEE Transactions on Ultrasonics, Ferroelectrics, and Frequency Control*, vol. 67, no. 12, pp. 2510–2518, 2020.
31. A. Van Den Oord, N. Kalchbrenner, and K. Kavukcuoglu, "Pixel recurrent neural networks," in *International conference on machine learning*, pp. 1747–1756, PMLR, 2016.